Delocalization and occupancy effects of $5f$ orbitals in plutonium intermetallics using L_3-edge resonant x-ray emission spectroscopy

C. H. Booth[a,*], S. A. Medling[a], Yu Jiang[a], E. D. Bauer[b], P. H. Tobash[c], J. N. Mitchell[c], D. K. Veirs[d], M. A. Wall[e], P. G. Allen[e], J. J. Kas[f], D. Sokaras[g], D. Nordlund[g], T.-C. Weng[g]

[a]*Chemical Sciences Division, Lawrence Berkeley National Laboratory, Berkeley, California 94720, USA*
[b]*Materials Physics and Applications Division, Los Alamos National Laboratory, Los Alamos, New Mexico 87545, USA*
[c]*Materials Science and Technology Division, Los Alamos National Laboratory, Los Alamos, New Mexico 87545, USA*
[d]*Manufacturing Engineering and Technologies Division, Los Alamos National Laboratory, Los Alamos, New Mexico 87545, USA*
[e]*Materials Science and Technology Division, Lawrence Livermore National Laboratory, Livermore, California 94550, USA*
[f]*Department of Physics, University of Washington, Seattle, WA 98195, USA*
[g]*Stanford Synchrotron Radiation Lightsource, SLAC National Accelerator Laboratory, Menlo Park, CA 94025, USA*

Abstract

Although actinide (An) L_3-edge x-ray absorption near-edge structure (XANES) spectroscopy has been very effective in determining An oxidation states in insulating, ionically-bonded materials, such as in certain coordination compounds and mineral systems, the technique fails in systems featuring more delocalized $5f$ orbitals, especially in metals. Recently, actinide L_3-edge resonant x-ray emission spectroscopy (RXES) has been shown to be an effective alternative. This technique is further demonstrated here using a parametrized partial unoccupied density of states method to quantify both occupancy and delocalization of the $5f$ orbital in α-Pu, δ-Pu, $PuCoGa_5$, $PuCoIn_5$, and $PuSb_2$. These new results, supported by FEFF calculations, highlight the effects of strong correlations on RXES spectra and the technique's ability to differentiate between f-orbital occupation and delocalization.

Keywords: actinide alloys and materials, superconductors, heavy fermions, plutonium, XANES, RXES

1. Introduction

A hallmark of strongly-correlated electron behavior in lanthanide-based materials is the partial $4f$-orbital occupancy, n_f, caused by strong interactions between localized f electrons and delocalized electrons in energetically nearby orbitals, such as the conduction band [1]. Lanthanide L_3-edge x-ray absorption near-edge structure (XANES) spectroscopy has been very successful in providing a bulk-sensitive, accurate, and relatively routine method for measuring n_f [2, 3, 4, 5, 6, 7, 8]. Unfortunately, this method is not very effective when applied to actinide materials due to a decrease in the energy separation of relevant $5f$ spectroscopic features (typically $\lesssim 5$ eV [9, 10] for light actinides and ≈ 10 eV for the lanthanides) and an overall decrease in the intrinsic spectral resolution from the decreased $2p_{3/2}$ core hole lifetime (about 8-10 eV for the light actinides, compared to 3-4 eV for the lanthanides [11]). In addition, since $5f$ orbitals are generally more delocalized than $4f$ orbitals, the ability of the $5f$ orbital to screen the core hole can vary from sample to sample, further confusing the interpretation of actinide L_3-edge XANES spectra. Here, we demonstrate the use of the resonant x-ray emission spectroscopy (RXES) technique from the L_3 edge, which has been used successfully on a range of intermediate-valent lanthanide intermetallics [12, 13, 14, 15], to help overcome these limitations in plutonium intermetallic compounds.

*Corresponding author.
Email address: chbooth@lbl.gov (C. H. Booth)

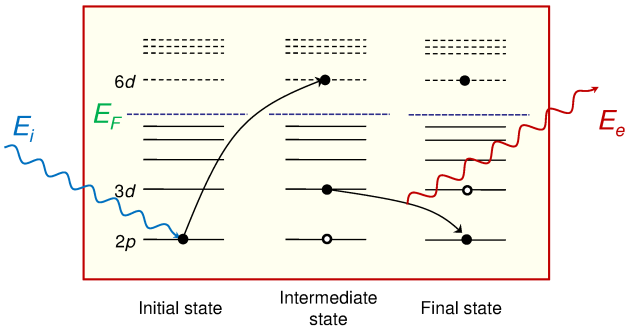

Figure 1: Schematic of the RXES process. RXES is a two step process involving an excitation by an incident photon of energy E_i out of the initial, or ground, state of, for example, a $2p$ electron to a state above the Fermi level, denoted here as a $6d$ state. The second step involves the decay of a $3d$ electron that fills the $2p$ hole and emits a photon with energy E_e.

Although the fundamental limitations on conventional XANES spectroscopy likely will always forbid its use in determining f-orbital occupancy in actinide intermetallics, the RXES technique and related techniques offer ways to obtain the same information with higher resolution. In particular, one way to improve the lanthanide (Ln) and actinide (An) L_3-edge spectra is to measure the $L_{\alpha 1}$ x-ray emission line with high resolution as the incident photon energy, E_i, is scanned across the L_3 edge [12]. This technique, illustrated in Fig. 1, separates the L_3 x-ray absorption/emission process into three parts: the ground , intermediate, and final states. The absorption process begins when the incident photon is absorbed by a $2p_{3/2}$ core electron, giving an intermediate state with a $2p$ core hole and an extra electron in a previously empty or partially empty orbital, denoted in the figure as a $6d$ orbital. This intermediate state is the final state of a conventional absorption process, where the broadening of the L_3-edge absorption spectra is limited by the $2p$ core hole lifetime. Continuing from the intermediate state, one relaxation path is a decay of a $3d$ electron, filling the $2p$ hole and leaving behind a $3d$ hole and a characteristic x-ray. It has been shown that if one measures this characteristic x-ray with sufficiently high resolution, the final spectral broadening is dominated by the lifetime of the $3d$ core hole, rather than the initial $2p$ core hole, significantly sharpening the spectra [12]. If one measures the emitted photon only at the energy of peak emission, the spectrum as a function of E_i is essentially a conventional XANES spectrum, but with higher energy resolution. Such spectra have been given different names, such as high-energy resolution fluorescence detection (HERFD) [16], but here we will refer to them simply as high-energy partial fluorescence yield (PFY) spectra. More information can be obtained by performing RXES, where one measures the emission both as a function of the emission energy, E_e, and of E_i. Such data are usually reported as a function of E_i and $E_t = E_i - E_e$, since E_t is the amount of energy transferred to the system in the final state and is therefore the change in energy of the system relative to the ground state. Several excellent reviews describing the RXES technique are available in the literature [17, 18, 19]

Since different oxidation states in otherwise similar bonding environments should be separated by about 5 eV [10], the broadening expected from a $3d$ core hole (about 4 eV) should be sufficiently narrow to see features associated with different oxidation states. This fact has been successfully exploited in RXES studies of An coordination compounds [20, 21], and a recent null result in a search for different oxidation state components in Am metal under applied pressure [22] has helped limit theoretical models [23] of the observed structural transitions in that element [24].

Most recently, our RXES study of some uranium and plutonium intermetallics found that, indeed, features in the RXES spectra were consistent and well described by intermediate valent, or multiconfigurational, ground states, especially in two forms of elemental plutonium, α-Pu and δ-Pu [25]. We will expound on those results below and outline some improved analysis techniques that are applied to the previous RXES data, as well as to data from two new samples, the Pu-based 115 superconductors, $PuCoGa_5$ [26] and $PuCoIn_5$ [27].

2. Experimental

A description of the sample synthesis and preparation for the α-Pu, δ-Pu, $PuCoGa_5$, $PuCoIn_5$, and $PuSb_2$ samples has been described previously [25]. The $PuO_{2.06}$ sample started from a well characterized stock [28] that was subsequently calcined and delivered in a pure helium atmosphere, then handled and epoxied in dry inert atmospheres (He and Ar). Given this treatment, the uptake of water by the oxide should be negligible. X-ray diffraction indicated clear and sharp PuO_2 peaks with no amorphicity. In particular no Pu_2O_3 peaks were observed. Further details regarding this sample have been previously reported [28].

Most of the measured samples are solid crystalline material, typically measuring about 2 mm on a side. The exception is the $PuO_{2.06}$ sample, which was encapsulated in Stycast 1266 epoxy. No special treatments were performed on the samples to prepare for the x-ray measurements, except that samples were chosen that had accessible flat surfaces to use as the incident plane for the x-rays. Each sample was loaded into a specially designed, triply-contained slotted aluminum holder with Kapton windows. The primary container was loaded under an inert atmosphere for the α-Pu, δ-Pu, and $PuO_{2.06}$ samples.

RXES data were collected at room temperature on beamline 6-2 at the Stanford Synchrotron Radiation Lightsource (SSRL) with a 7-crystal Johann-type spectrometer [29] using Ge(777) crystals and a Si(311) monochromator. Total instrumental broadening was determined to be 1.7 eV by measuring the direct scattered beam. Beam size was 500 $\times$ 200 μm. The monochromator energy calibration was performed by setting the first inflection point of the Pu L_3-edge absorption data collected on a PuO_2 reference powder to 18062.3 eV [10]. Other experimental details have been published previously [25]

3. Methods

A number of improvements have been made since the initial RXES report on elemental Pu and $PuSb_2$ [25]. First, a self-absorption correction has now been employed. This correction is obtained from a simple extension to the correction typically applied to conventional XANES data [30], namely, that the corrected normalized emission flux, I'_e, is given by

$$\frac{I_e^{\rm actual}(E_i,E_e)}{I_0(E_i)} = \frac{I_e^{\rm measured}(E_i,E_e)}{I_0(E_i)} \times \frac{\beta\frac{sin\theta_i}{sin\theta_e}+\gamma}{\beta\frac{sin\theta_i}{sin\theta_e}+\gamma'+1-\frac{I_e(E_i,E_e)}{I_e(E_i^+,E'_e)}},$$

where the sample is considered to be infinitely thick and the normalization is chosen as the emission flux at the peak emission energy, $E^+_{\rm emis}$, and at the last incident energy collected, E_i^+, which assumes the data were collected over a short energy range. The angle of the incident and the emitted photons, θ_i and θ_e, are measured relative to the sample surface, and are generally taken to be 45°. In addition, $\beta = \mu_t(E_{\rm emis})/\mu_a(E_i^+)$, $\gamma = \mu_b(E_i)/\mu_a(E_i^+)$, and $\gamma = \mu_b(E_i^+)/\mu_a(E_i^+)$, where $\mu_t(E)$ is the total absorption coefficient at energy E, $\mu_a(E)$ is the absorption from just the edge (atom) of interest (*eg.* from the Pu L_3 with the M-edge contributions removed), and $\mu_b(E)$ is the contribution from all background absorption processes (*eg.* the Pu M-edges and the absorption due to Sb in $PuSb_2$). The absorption coefficients are calculated using the known chemical formula and the McMaster Tables [31]. For other approximations used in this formula, refer to the FLUO documentation [30].

The second improvement to the RXES data analysis is that fits are now made using an adaptation to the Kramers-Heisenberg formula describing the full, 2-dimensional E_i, E_t plane of the normalized measured

emission intensity (see, for example, Ref. [32, 33]):

$$I_e(E_i, E_t) = \sum_f \sum_i \int d\epsilon\ \eta(\epsilon) \frac{\langle f|T_2|i\rangle^2 \langle i|T_1|g\rangle^2}{(E_{gi} - \epsilon + E_i)^2 + \Gamma_i^2/4} \times \frac{\Gamma_f/(2\pi)}{(E_{if} - \epsilon + E_t)^2 + \Gamma_f^2/4}, \quad (1)$$

where the sum is over excitations from the ground state, g, to the intermediate state, i, which decays to the final state f, and the unoccupied partial density of states (upDOS), $\eta_i(\epsilon)$, is normalized to include constant effects such as detector solid angle and transition efficiencies, etc. The energies E_{gi} and E_{if} are the differences in energy between the ground and the intermediate state, and the intermediate and the final state, respectively. For this work, the primary transition from the ground state to the intermediate state is the dipole transition from the $2p_{3/2}$ shell to the $6d$ manifold above the Fermi energy, E_F. Although a $2p_{3/2} \rightarrow 7s$ is allowed, the transition probability compared to that into a d state is only about 2% [34], and the available density of states in these compounds is very small near E_F, so these transitions can be neglected. Quadrupole transitions directly into the f states are possible, and indeed have been observed in some materials [12], but FEFF9 calculations (discussed further below) indicate they have a negligible contribution here.

As for the intermediate-to-final state transition, the spectrometer is tuned such that only the $3d_{5/2} \rightarrow 2p_{3/2}$ transition, that is, the $L_{\alpha 1}$ fluorescence, is measured. Therefore, under these assumptions one can assume the matrix elements T_1 and T_2 for the individual state transitions within a given material are equal, and one can simplify Eq. 1 to

$$I_e(E_i, E_t) \propto \int d\epsilon\ \frac{\eta(\epsilon)}{(E_{gi} - \epsilon + E_i)^2 + \Gamma_i^2/4} \times \frac{\Gamma_f/(2\pi)}{(E_{if} - \epsilon + E_t)^2 + \Gamma_f^2/4}, \quad (2)$$

where for multiple intermediate states, and E_{gi} and E_{if} are now energy offsets corresponding to the lowest energy excitation above the Fermi level.

Using Eq. 2, it is possible to fit to RXES data with E_{gi}, E_{if}, Γ_i, Γ_f, and $\eta(\epsilon)$ as the fit parameters. Short of deconvolving Eq. 2 to obtain $\eta(\epsilon)$ directly, one can parametrize $\eta(\epsilon)$ using some knowledge of the material. As discussed previously [25], when an f-electron intermetallic is in an intermediate valent state, the f contribution to the ground state will be a quantum mechanical mixture of various possible f configurations, such as

$$|f\rangle = c_4|f^4\rangle + c_5|f^5\rangle + c_6|f^6\rangle,$$

where c_i^2 give the probability of finding the system in any one configuration f^i. When the core hole is created in the intermediate state, the Coulomb interaction between the hole and these f configurations splits the degeneracy [35]. Since each configuration has a different number of electrons, they will each screen the core hole differently, giving rise to an energy splitting in the intermediate and final states. This splitting is reflected in the empty d states, that is, in $\eta(\epsilon)$. A reasonable parametrization of $\eta(\epsilon)$ is therefore a combination of a Gaussian to represent the excitations into the comparatively discrete empty $6d$ states and a broadened step function to represent the continuum of states. Each potential configuration is then represented by this combination of a Gaussian and the step function.

In the fits reported below, $\eta(\epsilon)$ is parametrized with each of three configuration contributions, p_1, p_2, and p_3, split by a constant energy of 5.25 eV (corresponding to $\Delta n_f = 1\ e^-$) and given by a Gaussian of width Γ_p and of height p/s relative to the continuum step.

Note that in removing the sum over matrix elements in going from Eq. 1 to Eq. 2 makes explicit certain assumptions regarding multiconfigurational states. in particular, the configuration splitting is assumed to be the same in the intermediate state and in the final state in the fits reported below. Related to this

Table 1: RXES fit results. Peak separation held at 5.25 eV. Three peaks, p_1, p_2, and p_3, were varied in the parametrized upDOS, each consisting of a smoothed step function plus a Gaussian. The reported n_f assumes the full amplitude of each of these peaks accounts for a configuration fraction for the f^6, f^5, and f^4 weight respectively, with only th $PuO_{2.06}$ sample also including p_4 peak for a f^3 contribution. "p/s" is the relative amplitude of the Gaussian to the step. Reported errors for most parameters are based on the number of free parameters and the covariance matrix, and represent the random errors. The reported error on the f-orbital occupancy is based on the estimated absolute, systematic error on the configuration fractions. Absolute errors are estimated to be about 0.1 for each configuration fraction. For comparison, note that the nominal n_f of $PuO_{2.06}$ is 3.88.

compound	E_{gi}	Γ_i	E_{if}	Γ_f	p/s	Γ_p	$p_1(\%)$	$p_2(\%)$	$p_3(\%)$	$p_4(\%)$	n_f
α-Pu	18061.4(3)	8.5(1)	3779.9(3)	2.1(1)	1.65(5)	3.1(1)	31(3)	56(4)	13(3)	-	5.2(1)
δ-Pu	18059.8(3)	8.6(1)	3778.7(3)	2.1(1)	1.41(6)	3.2(2)	46(3)	46(3)	8(2)	-	5.38(15)
$PuCoGa_5$	18060.3(2)	8.5(1)	3779.9(1)	3.2(1)	1.87(7)	2.4(4)	9(2)	62(2)	29(2)	-	4.8(1)
$PuCoIn_5$	18059.9(1)	8.1(1)	3779.3(1)	3.0(1)	1.96(6)	2.4(3)	2(1)	77(2)	21(2)	-	4.8(1)
$PuSb_2$	18057.2(1)	8.0(1)	3775.4(1)	2.8(1)	2.54(6)	2.1(1)	7(1)	78(1)	15(1)	-	4.9(1)
$PuO_{2.06}$	18059.5(1)	9.3(1)	3779.3(1)	1.7(1)	1.82(7)	3.6(3)	2(1)	13(2)	80(3)	4(2)	4.1(2)*

assumption is that other, higher-order, sources of off-diagonal transitions, such as a two-electron transition involving a change in the f configuration between the intermediate and final states, are also ignored in the fits. In each case, satellite peaks would appear near the main resonance in the RXES spectra at a constant E_i that are not observed, justifying these assumption.

4. Results

4.1. RXES measurements and fit results

The previous method [25] of fitting each trace as a function of transfer energy at a fixed incident energy required approximately 10 fitting parameters for each incident energy scan. Even though some could be fixed across the entire data set, this amounted to in excess of 500 parameters for each RXES spectrum. The new method has much less flexibility, with only about 10 parameters allowed to vary for the entire 2-dimensional spectrum, without a significant decrease in the quality of fit. The weakness of the technique from a fitting point of view is simply one of choosing an appropriate lineshape, for which there is little *a priori* knowledge. If calculational methods could be improved, it could be possible to base a lineshape on a theoretical calculation, but that situation does not yet exist.

Examples of the data and fit results are reported for $PuSb_2$ (Fig. 2) and $PuCoIn_5$ (Fig. 3). The best fit for the unoccupied partial density of states summed over the three configuration lineshapes is given in Fig. 4. The fit results are summarized in Table 1.

It is important to note that at this point in this article, we have not yet assigned any particular f configuration to the reported fractions p_1, p_2, and p_3 in Table 1. To that end, we first consider data on the $PuO_{2.06}$ sample to calibrate the threshold energies for a localized f material, and as a test of the method for providing accurate f occupancies. By comparison, the threshold E_{gi} energies are nearly constant across the series, with only that of $PuSb_2$ deviating appreciably. A similar situation exists for E_{if}. In the fits, these energies corresponds to the lowest energy peak in the upDOS, which is ideally due solely to the f^6 configuration. The peak width Γ_i is very nearly the expected value from the $2p_{3/2}$ core hole lifetime of 8.7 eV. Meanwhile, the fitted peak width Γ_f is typically somewhat smaller than that expected from the $3d$ core hole life times ≈ 4.1 eV. We do not currently offer a rationalization for this fact. Note that these widths are different than those reported previously in these materials due to the recent application of a self-absorption correction to these data (Sec. 3), and also that these widths include the total instrumental broadening (Sec. 2). In any case, the p_3 peak must be assigned to the f^4 configuration in $PuO_{2.06}$. The other peaks, p_1 and p_2, are then fixed at -10.5 eV and -5.25 eV relative to p_3 and corresponding to $+2$ e^- and $+1$ e^- differences in their electron count, that is, to the f^6 and f^5 configurations, respectively.

The excess oxygen in the $PuO_{2.06}$ sample implies possible f^3 and/or f^2 contributions. Fits including an f^2 contribution indicated non was present, although some f^3 may be present. The fits in Table 1 therefore

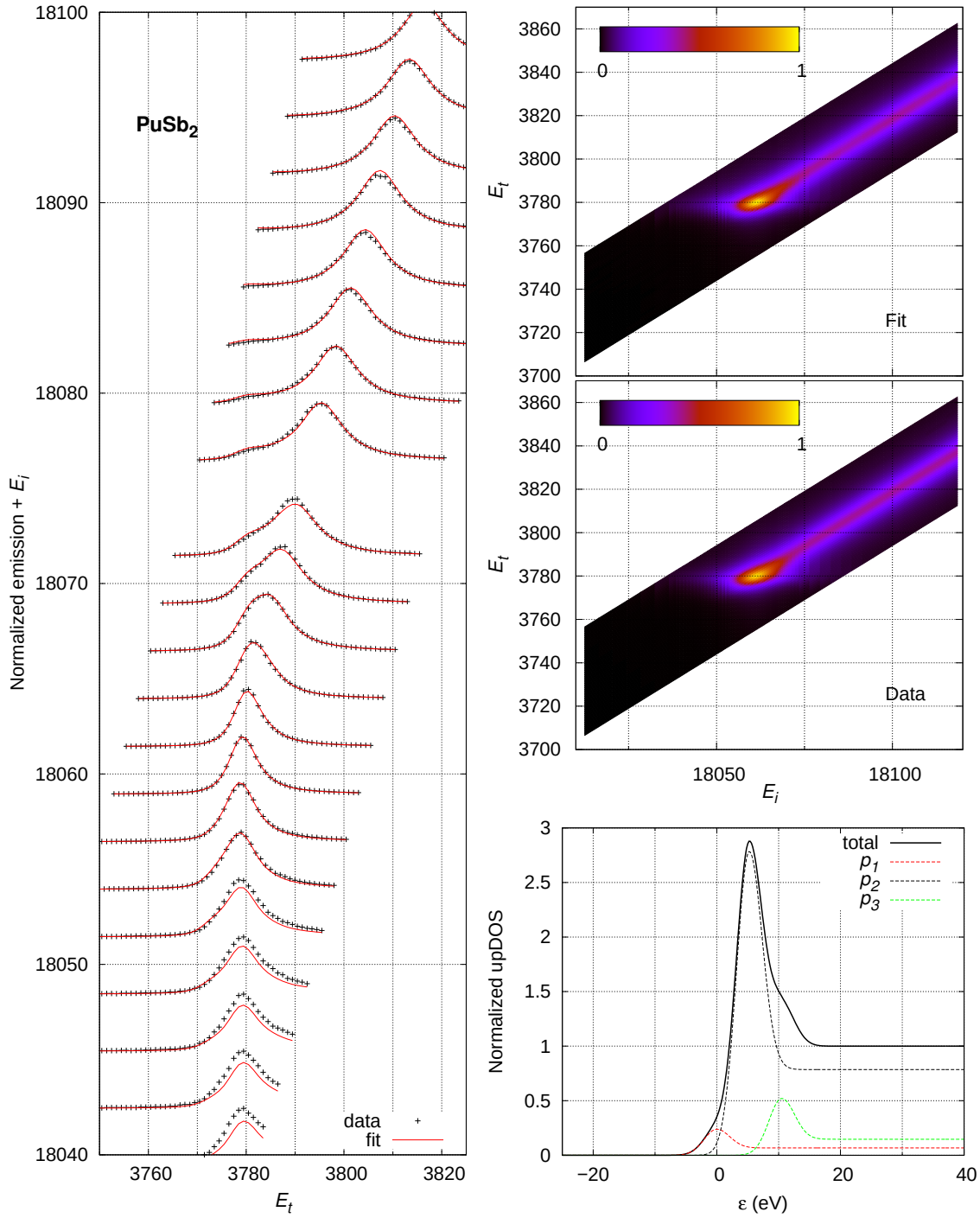

Figure 2: RXES data and fit results for $PuSb_2$. The data and fits are displayed in two different ways. The left panel shows a selection of constant-E_i cuts as a function of E_t. Each cut is normalized to that cut's maximum emission so that data below the main threshold energy ≈ 18060 eV, where the emission flux is comparatively quite low, is visible on the same scale as data above this energy. Data are offset by that scan's E_i. On the right are the 2-dimensional color plots, followed by the fitted parametrized $\eta(\epsilon)$ (upDOS) with its individual components.

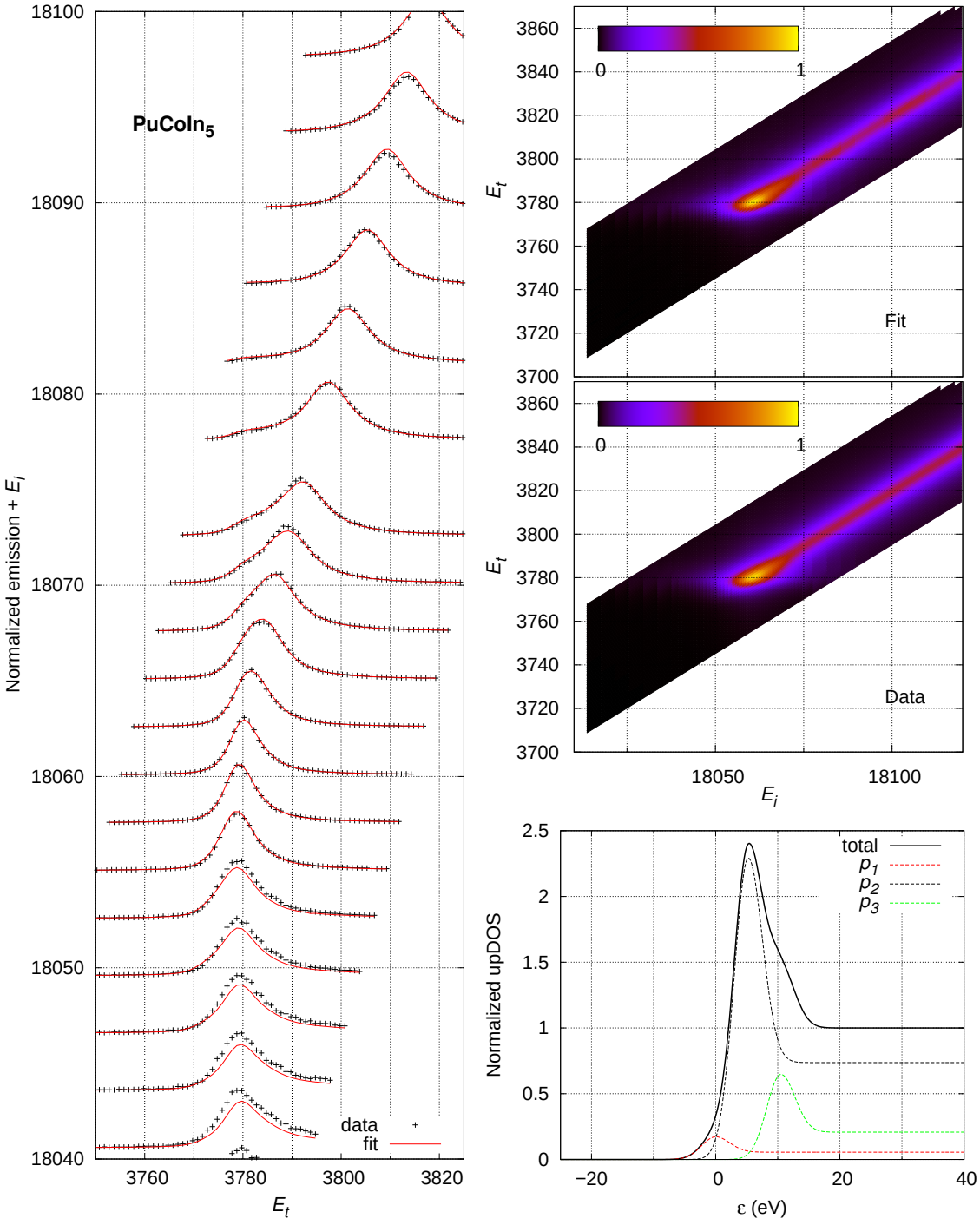

Figure 3: RXES data and fit results for $PuCoIn_5$. See Fig. 2 for a description.

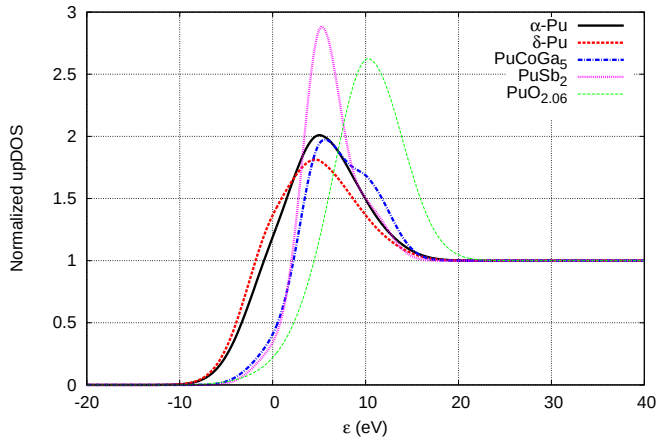

Figure 4: The upDOS obtained in the parametrized fits to the RXES data for all measured samples.

include a fourth peak, p_4, to attempt to account for an f^3 contribution. The estimated $n_f = 4.1(2)$ is consistent with the expected n_f from the oxygen stoichiometry, and the potential presence of pentavalent Pu (f^3) is consistent with recent work on oxidized forms of PuO_2 [36, 37].

In order to make peak assignments for the other measured materials, there are some important points to consider. Foremost is that the f^4 (highest energy) peak energy can't be much higher than that of PuO_2, since the f's must be fairly localized already in PuO_2 (FEFF calculations given below indicate an f peak in the upDOS similar in width to that of $PuCoIn_5$, as well as a similar Fermi energy), and any delocalization would only increase the threshold. For most of the other Pu materials reported here, the E_{gi} and E_{if} energies are similar to that of $PuO_{2.06}$, and the peak configuration assignments are made accordingly. The exception is $PuSb_2$, which apparently does have a more strongly localized f orbital judging from both its experimentally measured intense and narrow main emission feature and its shifted threshold energy relative to all other samples. For these reasons, the main peak in $PuSb_2$ is associated with a localized f^5 configuration. The reported n_f's in Table 1 are therefore all made with the p_1, p_2, and p_3 peaks assigned to the f^6, f^5, and f^4 configurations, respectively.

4.2. PFY measurements and FEFF Calculations

In addition to the full RXES spectra, it is important to consider some basic simplifications to these spectra. Figure 5(upper) shows data for each measured sample where the spectrometer was set to only measure at a single emission energy that corresponds to the E_e at peak resonance for the Pu L_3 edge. As mentioned previously, we refer to such a cut as PFY data. If one instead integrates over the whole emission peak at a given E_i, then one obtains the more conventional low-resolution total fluorescence yield (TFY) XANES spectra, which are shown for comparison in Fig. 5(lower). The enhancement of the spectra in Fig. 5(upper) is obvious and substantial, and helps emphasize the sizable energy shift between the different samples and the changes in the main resonance amplitude, a.k.a the white line height.

As was noted previously [25], conventional XANES spectra (and by extension, PFY spectra) cannot be used to determine absolute f configuration fractions in uranium and plutonium intermetallics because the observed energy shifts of the L_3 edge may be due to either a change in f occupancy, a change in f localization, or some combination of the two. This situation is in contrast to that in Ln intermediate valent systems because the f band remains narrow, and thus effectively screens the $2p_{3/2}$ core hole, more or less equally for all materials. However, the f orbital bandwidth can change significantly between different plutonium intermetallics; that is, the degree of f delocalization can change.

At the present time, there are no available methods for calculating RXES spectra for correlated f-electron systems, although some excellent codes do exist for materials that aren't dominated by electron correlations [38, 39]. Fortunately, the FEFF code (version 9.6.4) is capable of demonstrating the role of f

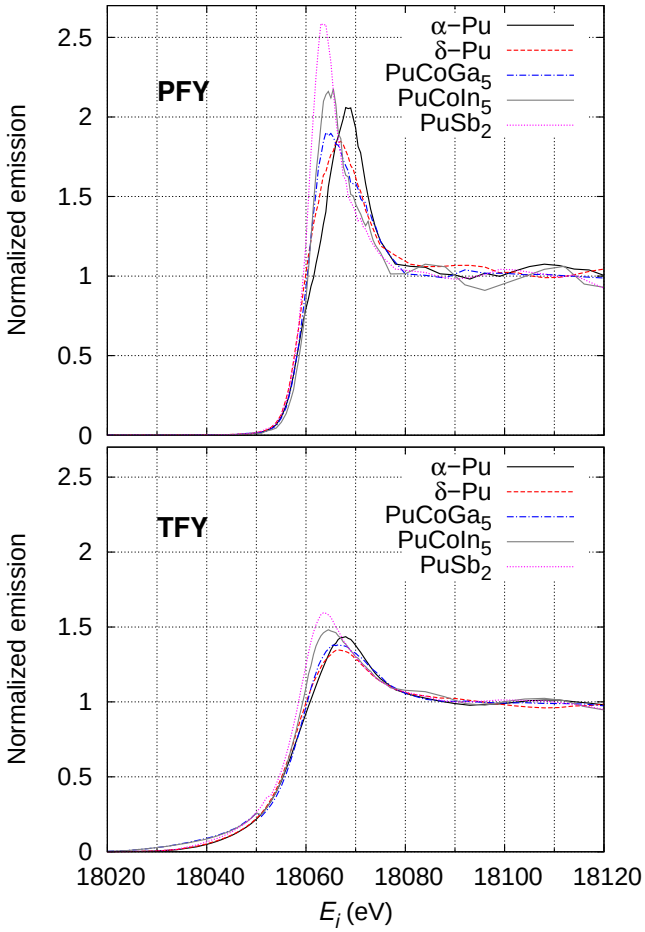

Figure 5: Experimental PFY and TFY results for all samples.

orbital delocalization in contributing to shifts in the threshold energy [40, 41]. Figure 6 shows the results from such *ab initio* calculations using the nominal crystal structures [26, 27, 42, 43, 44] and mostly default values for running the code, with a few exceptions. The cluster radius was chosen to be 6 Å after finding that the calculations for all samples were converged using this size. By default, FEFF freezes the f-occupancy at a nominal value, which produces some sizable errors in the Fermi energy estimates, so the calculations reported here allow the f-occupancy to vary. Each calculation used the Hedin-Lunqvist potential. FEFF applies a default core-hole broadening of 8.7 eV for a Pu L_3-edge absorption calculation. The calculations in Fig. 6(upper) are narrowed from this value by 2 eV in order to simulate the effects of taking a PFY cut through the RXES plane, while the calculations shown in Fig. 6(lower) use the default value to simulate conventional XANES data and the TFY integrations of the RXES data. Although narrowing by 4 eV for the PFY spectra produces better agreement between the white-line heights in the calculations compared to the data, a 2 eV narrowing was chosen because FEFF produces much sharper spectral features elsewhere in the spectra that obscure the main comparisons discussed below, emphasizing that comparisons between these calculations and the data should only be made qualitatively.

A clear shift in threshold energy is observed in these calculations, as indicated by the shift in the main edge, but also from the position of the peak absorption. This shift is reflected in the Fermi level shift, but not in the amount of charge transfer or in the f occupancy (Table 2). The reason for this shift illustrates that An f electrons can experience significant delocalization, which can reduce the core-hole screening and hence

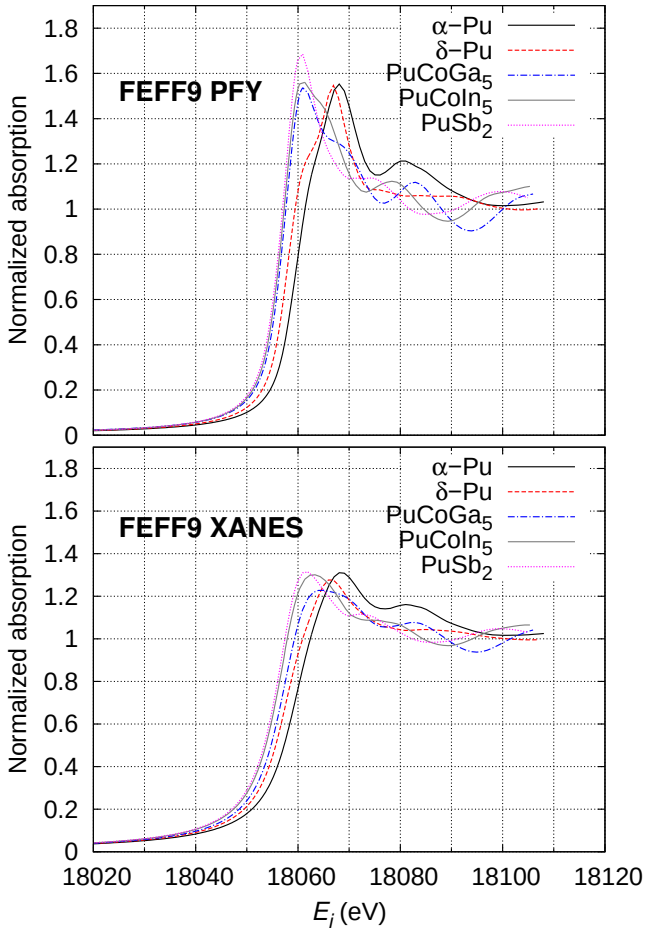

Figure 6: Calculations of the PFY and XANES using FEFF 9.6.4, as described in the text. The XANES calculations use the default core-hole broadening; PFY spectra are narrowed by 2 eV.

shift the Fermi level. This situation is illustrated in Fig. 7(upper), which shows a systematic sharpening of the f density of states going from α-Pu to $PuSb_2$, exactly following the trend in E_F. This sharpening reflects the systematic localization of the f electron. For comparison, the f density of states in Yb calculations are always only about 0.2 eV full width at half maximum. In contrast, the d band extends over many eV [Fig. 7(lower)], and shows no obvious correlation with the energy shifts. These calculations therefore demonstrate that one can achieve edge shifts without a change in the f-occupancy in these compounds, as discussed previously from a purely experimental point of view [25].

The comparison between the calculations (Fig. 6) and the actual data (Fig. 5) allows for other interesting conclusions. First, the shift of the main edge in the calculations is much smaller in the actual data. Given the similarity in the shift of the white line position, this may be indicative of the competing effects of f orbital delocalization and occupancy. Another striking feature is the difference in amplitude of the white line features. Related to this observation is the generally more strongly modulated character of the calculated XANES, despite the smaller amplitude of the white line. At least part of the explanation for these differences lies in the lack of f/d electronic correlations in the calculation, which should produce a stronger f/d hybridization, and therefore a stronger peak in the d density of states at the Fermi level.

Table 2: Charge transfer (CT), Fermi energy (E_F), and f-occupancy (n_f) in the final state from FEFF calculations. Note that the final state starts from the so-called "final state rule" [45], which includes an extra electron in the f orbital to balance the core hole, which we denote here as n_f^*.

compound	CT	E_F (eV)	n_f^*
α-Pu	0.242	-14.737	6.605
δ-Pu	-0.067	-11.692	6.727
$PuCoGa_5$	0.258	-10.274	6.663
$PuCoIn_5$	0.309	-9.231	6.697
$PuSb_2$	0.129	-8.057	6.736

5. Discussion

Given the results of the calculations, it is clear that one cannot use the Pu L_3 edge position to determine f occupancy. One instead must rely on the effect of a split peak of the main absorption line. The basic idea is that states near the Fermi level are sharp in these materials, enhanced to some degree by electron correlations. Assuming that the f state is an intermediate valence state, as discussed in Sec. 3, the final state $2p$ core hole will split these states. Once these states are split, their absolute energy positions are less important for determining n_f, since n_f may be determined by the relative weight of each configuration fraction.

There are three important caveats to this technique. The first is made clear by the FEFF calculations. Although these calculations are only in rough qualitative agreement with experimental data, details in the d band could be mistaken for peaks split by the different f configurations. This concern is partially mitigated by the clear enhancement of the white line feature in experiments relative to the calculation, as well as the overall smearing out of details in other parts of the spectrum. Based on these facts, we estimate that the error in any particular configuration fraction remains below the 0.1 estimate reported earlier [25].

Regarding the absolute error estimate of 0.1, which was based on the lack of knowledge about the exact lineshapes, we note that this estimate is consistent with discrepancies between measurements using different techniques in the literature. For instance, using $YbAgCu_5$, $YbInCu_5$, and $YbAl_3$ for comparisons, estimates of Yb valence using L_3-edge XANES [4, 5] are generally consistent with photoemission (as long as surface effects are reduced [46, 47]), and M-edge studies [47]. The role of the excited state core-hole should be different in these measurements, yet they all have results within about 0.1 electrons for the valence of specific materials. Theoretical comparisons are difficult in these systems due to the many-body nature of the ground states, but in small molecules where electron correlations are important, high-levels of theory are applicable, such the multiconfiguration Complete Active Space Self Consistent Field (CASSCF) method. In these cases, estimated valences are within 0.05 electrons in a variety of Yb organometallic compounds [6, 48]. However, without many-body calculations on plutonium compounds, the role of the final-state core hole will remain unclear, and while all experimental indications are consistent with a 0.1 electron absolute error, it remains possible that this error estimate could be somewhat too small.

The second important caveat is that it isn't always clear when one expects a split state. In order to split the f electrons in an intermediate valent state, the Coulomb interaction $U_{\bar{p}f}$ between the core hole $\bar{p}$ and an f electron has to be larger than the binding energy of the intermediate valence state [35]. In Ln materials, the strong localization of the f electrons guarantees a large $U_{\bar{p}f}$, thereby enabling a split peak in all known Ln intermediate valence materials at the Ln L_3 edge. In contrast, this splitting condition is typically not met in transition metal systems, and no split peaks are observed (energy shifts are observed instead) [49]. Actinides can potentially exhibit either kind of behavior.

The third and final caveat is that although multiple features corresponding to different state configurations are observed in some compounds, they are sometimes only observed as an enhanced broadening of the emission spectrum. In this analysis, we assume three features are present in an effort to treat all data on the same footing. This treatment is justified by the small peak widths consistently observed in the fit results.

The primary purpose of this article is to expound upon the RXES method for obtaining information about the f electronic structure using Pu L_3-edge excitations. As such, data are presented that were first

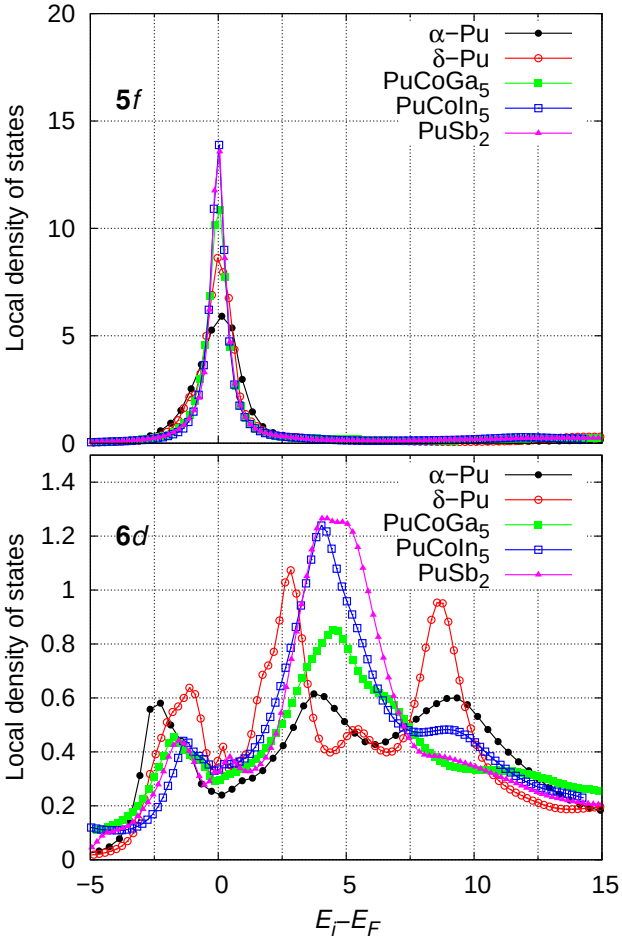

Figure 7: The unoccupied local partial density of states functions for (upper) f and (lower) d states. These states are artificially broadened using a constant imaginary component of 0.2 eV. Note that in the final XANES calculation, core hole broadening of several eV is applied.

reported previously [25], as well as data on two currently relevant samples, namely, the 115 superconductors. The former are presented to highlight improvements, while the latter were chosen to extend the literature base and further the knowledge of the electronic structures in this important class of material.

The improvements to the technique have allowed for better fit results over the entire range of collected data while greatly decreasing the number of fit parameters. The self-absorption correction has served to properly sharpen the spectra taken above the threshold energy, although the change in n_f estimates is small. It should be noted that the primary affect of the self-absorption correction on these fits and those reported previously is the decreased intermediate and final state widths, Γ_i and Γ_f.

The biggest success of the new methods is providing a proper fit of the spectra from $PuSb_2$. The previous method of fitting each incident energy scan individually did not provide a wholly unambiguous result, since the peak in the XES scans appeared to shift uncharacteristically as the incident energy increases in the threshold vicinity. This shift is now understood in terms of a nearly mono-configurational f^5 state and a very sharp resonance.

Through comparison with the FEFF calculations (Fig. 6), the PFY results on the Pu 115 superconductors (Fig. 5) indicate that $PuCoIn_5$ has a narrower f band than that of $PuCoGa_5$, consistent with recent calculations [50]. On the other hand, the f-band of δ-Pu is rather similar to that of $PuCoGa_5$. The most surprising result is the apparently large p_3 peak fraction (Table 1), consistent with an f^4 content between

20% and 30%, while the small f^6 content is consistent with zero ($< 10\%$). This combination gives an $n_f = 4.8 \pm 0.1$ for both 115 samples, in contrast to recent calculations that indicate more f^6 character and an n_f resembling that of δ-Pu [51], although the RXES results are qualitatively consistent in the presence of a mixed valence state and similarity of the f-band width to that of δ-Pu.

There are potential reasons why weight may exist in any of the peaks p_1, p_2, or p_3 that does not correspond to a particular ground state f configuration, other than spurious features in the d band mentioned earlier. One possibility is a heavily oxidized surface of the sample. We do not, however, believe this reason is justified here: While one might be tempted to assign a portion of p_3 to an oxidized surface, there is no indication from local structure measurements that such a phase exists, especially at such abundance. It is possible that self-irradiation damage somehow plays a role, since this structure is known to self-damage quickly, even at room temperature, with $\approx 25\%$ of the atoms displaced or distorted within a year of their last anneal [52]. This damage rate is in contrast to the lack of damage developing at room temperature due to annealing in δ-Pu [53, 54, 55], a situation that is linked to bond strength; hence, the Debye temperature is a qualitative indicator. In this sense, both α-Pu ($\Theta_D \approx 150$ K [56]) and δ-Pu ($\Theta_D \approx 100$ K [57]) have relatively low Debye temperatures, and so any damage will anneal out at room temperature easier than in $PuCoGa_5$ ($\Theta_D \approx 248$ K [58]), $PuCoIn_5$ ($\Theta_D \approx 203$ K [25]), or $PuSb_2$ ($\Theta_D \approx 255$ K [25]). With this difference in mind, it seems reasonable to be concerned that radiation damage could inflate p_3 over that of the ground state. It should be noted, though, that this conclusion would be inconsistent with the observed increase in magnetic moment with radiation damage in both δ-Pu [54] and $PuCoGa_5$ [59], which is consistent with a more localized f^5 configuration, not more f^6 weight.

As a final note regarding reliability, it must be stressed that it remains possible that an unusually large feature exists in the d band that is not related to configuration splitting in the excited state, and could therefore skew the RXES results. We do not have any evidence of such a feature at this time, as so maintain our current estimate of 0.1 as the systematic error on any one configuration fraction.

Bearing these potential errors in mind, one can make several useful observations about the measured materials based on the RXES data. Continuing with the superconductors, despite the potentially inflated f^4 configuration fraction, the results indicate very little weight at the p_1 peak position (f^6 configuration fraction), which cannot be easily ascribed to any known systematic errors. If one considers all of the weight in the p_3 peak to be due to some systematic error, the *upper bound* for n_f is 5.24 and 5.14 for $PuCoGa_5$ and $PuCoIn_5$, including the potential systematic occupancy error of 0.1 e^-.

A great advantage of these techniques is that an experimenter can deconvolve the competing effects of f-orbital occupancy and delocalization through the observation of split peaks and energy shifts. Such effects help explain the relatively large energy shift of about -5 eV in the $PuSb_2$ conventional XANES spectrum relative to that of α-Pu [25] and in the PFY spectrum reported here (Fig. 5), despite a difference of only -0.3 e^- in n_f, where one would otherwise expect an least a positive difference in the f occupancy based on the energy difference. Comparing to the FEFF calculations (Fig. 6), one can see that the bulk of the energy shift is due to the strong localization of the f band, which is even more localized than in PuO_2, as indicated by the negative energy shift of the threshold energies, E_{gi} and E_{if}. Although a substantial shift in the threshold energies is not observed for the 115 samples, the similarities between the PuO_2 and the 115 FEFF calculation and the data, as well as the overall increase and shift of the white line, indicate strong f localization in the superconductors, similar to PuO_2, but nevertheless intermediate between that of $PuSb_2$ and the two elemental plutonium samples.

The main conclusion reached for the superconductors is that the f^6 fraction is systematically decreasing going from δ-Pu to $PuCoGa_5$ and $PuCoIn_5$. This decrease in the f^6 contribution consequently indicates a moderately localized f orbital, weaker f hybridization with the conduction band, yet stronger correlations and more heavy-fermion-like electronic and magnetic behavior.

6. Conclusion

The RXES technique is powerful for obtaining information about the electronic structure of a material, especially in f-electron intermetallics where few alternative techniques exist. Moreover, the technique is

bulk sensitive and relatively easy to perform, assuming one has access to an appropriate, expertly-staffed beamline at a high-energy synchrotron source. For instance, recent improvements on beamline 6-2 at SSRL allow for a high quality full RXES spectra to be collected in about 45 min, which is now sufficiently fast to allow temperature dependent studies, or other studies where one may require many spectra.

Improvements to the data analysis and interpretation are still largely empirically based, and as such, data on more materials is still necessary. In particular, the apparent correlation between threshold energy and f-band localization should be further explored. While peak splitting and orbital occupancy effects are likely the most important effects in Pu spectra, a localization study will likely require uranium-based compounds, where delocalized f states should dominate, and neptunium-based compounds, which should exhibit crossover behavior.

7. Acknowledgments

This work was supported by the Director, Office of Science, Basic Energy Sciences (OBES), U.S. Department of Energy (DOE) under Contract No. DE-AC02-05CH11231. Work at Los Alamos National Laboratory was performed under the auspices of US. DOE, OBES, Division of Materials Sciences and Engineering. This work was also supported by DOE Grant DE-FG03-97ER45623 (JJK) and was facilitated by the DOE Computational Materials Science Network. X-ray absorption data were collected at SSRL, a national user facility operated by Stanford University of behalf of the DOE/OBES.

[1] N. E. Bickers, D. L. Cox, J. W. Wilkins, Self-consistent large-n expansion for normal-state properties of dilute magnetic alloys, Phys. Rev. B 36 (1987) 2036.

[2] G. H. Kwei, J. M. Lawrence, P. C. Canfield, Temeprature dependence of the 4f transition in ce3bi4pt3, Phys. Rev. B 49 (1994) 14708.

[3] Z. Hu, G. Kaindl, G. Meyer, X-ray absorption near-edge structure at the L(I-III) thresholds of Pr, Nd, Sm, and Dy compounds with unusual valences, JOURNAL OF ALLOYS AND COMPOUNDS 246 (1-2) (1997) 186–192. doi:10.1016/S0925-8388(96)02473-5.

[4] J. L. Sarrao, C. D. Immer, Z. Fisk, C. H. Booth, E. Figueroa, J. M. Lawrence, R. Modler, A. L. Cornelius, M. F. Hundley, G. H. Kwei, J. D. Thompson, F. Bridges, Physical properties of ybxcu/sub 4/ (x=ag, au, cd, mg, tl, and zn) compounds, Phys. Rev. B 59 (1999) 6855.

[5] E. D. Bauer, C. H. Booth, J. M. Lawrence, M. F. Hundley, J. L. Sarrao, J. D. Thompson, P. S. Riseborough, T. Ebihara, Investigation of Anderson lattice behavior in $Yb_{1-x}Lu_xAl_3$, Phys. Rev. B 69 (2004) 125102.

[6] C. H. Booth, D. Kazhdan, E. Werkema, M. D. Walter, W. W. Lukens, E. D. Bauer, Y.-J. Hu, L. Maron, O. Eisenstein, M. Head-Gordon, R. A. Andersen, Intermediate-valence tautomerism in decamethylytterbocene complexes of methyl-substituted bipyridines, J. Am. Chem. Soc. 132 (2010) 17537. doi:10.1021/ja106902s.

[7] Y. Utsumi, H. Sato, S. Ohara, T. Yamashita, K. Mimura, S. Motonami, K. Shimada, S. Ueda, K. Kobayashi, H. Yamaoka, N. Tsujii, N. Hiraoka, H. Namatame, M. Taniguchi, Electronic structure of Kondo lattice compounds $YbNi_3X_9$ (X= Al, Ga) studied by hard x-ray spectroscopy, Phys. Rev. B 86 (2012) 115114. doi:10.1103/PhysRevB.86.115114.
URL `http://link.aps.org/doi/10.1103/PhysRevB.86.115114`

[8] H. Fujishiro, T. Naito, D. Takeda, N. Yoshida, T. Watanabe, K. Nitta, J. Hejtmánek, K. Knížek, Z. Jirák, Simultaneous valence shift of Pr and Tb ions at the spin-state transition in $(Pr_{1-y}Tb_y)_{0.7}Ca_{0.3}CoO_3$, Phys. Rev. B 87 (2013) 155153. doi:10.1103/PhysRevB.87.155153.
URL `http://link.aps.org/doi/10.1103/PhysRevB.87.155153`

[9] B. Kosog, H. S. La Pierre, M. A. Denecke, F. W. Heinemann, K. Meyer, Oxidation state delineation via U L_{III}-edge XANES in a series of isostructural uranium coordination complexes, Inorg. Chem. 51 (2012) 7940–7944. doi:dx.doi.org/10.1021/ic3011234.

[10] S. D. Conradson, K. D. Abney, B. D. Begg, E. D. Brady, D. L. Clark, C. den Auwer, M. Ding, P. K. Dourhout, F. J. E. Faller, P. L. Gordon, R. G. Haier, N. J. Hess, R. F. Hess, D. W. Keogh, G. H. Lander, A. J. Lupinetti, L. A. Morales, M. P. Neu, P. D. Palmer, P. Paviet-Hartmann, S. D. Reilly, W. H. Runde, C. D. Tait, D. K. Veirs, F. Wastin, Higher order speciation effects on plutonium L_3 x-ray absorption near edge spectra, Inorg. Chem. 43 (2004) 116.

[11] O. Keski-Rahkonen, M. O. Krause, Total and partial atomic-level widths, Atomic Data and Nuclear Data Tables 14 (1974) 139–146.

[12] K. Hamalainen, D. P. Siddons, J. B. Hastings, L. E. Berman, Elimination of the inner-shell lifetime broadening in x-ray-absorption spectroscopy, Phys. Rev. Lett. 67 (20) (1991) 2850–2853. doi:10.1103/PhysRevLett.67.2850.

[13] C. Dallera, M. Grioni, A. Shukla, G. Vankó, J. L. Sarrao, J. P. Rueff, D. L. Cox, New spectroscopy solves an old puzzle: The kondo scale in heavy fermions, Phys. Rev. Lett. 88 (2002) 196403. doi:10.1103/PhysRevLett.88.196403.
URL `http://link.aps.org/doi/10.1103/PhysRevLett.88.196403`

[14] C. Dallera, E. Annese, J.-P. Rueff, A. Palenzona, G. Vankó, L. Braicovich, A. Shukla, M. Grioni, Determination of pressure-induced valence changes in ¡span class="aps-inline-formula"¿¡math¿¡mrow¿¡msub¿¡mrow¿¡mi mathvariant="normal"¿ybal¡/mi¿¡/mrow¿¡mrow¿¡mn¿2¡/mn¿¡/mrow¿¡/msub¿¡/mrow¿¡/math¿¡/span¿ by resonant inelastic x-ray

emission, Phys. Rev. B 68 (2003) 245114. doi:10.1103/PhysRevB.68.245114.
URL http://link.aps.org/doi/10.1103/PhysRevB.68.245114

[15] C. Dallera, M. Grioni, A. Palenzona, M. Taguchi, E. Annese, G. Ghiringhelli, A. Tagliaferri, N. B. Brookes, T. Neisius, L. Braicovich, α-γ transition in metallic Ce studied by resonant x-ray spectroscopies, Phys. Rev. B 70 (2004) 085112. doi:10.1103/PhysRevB.70.085112.
URL http://link.aps.org/doi/10.1103/PhysRevB.70.085112

[16] P. Glatzel, F. M. F. de Groot, O. Manoilova, D. Grandjean, B. M. Weckhuysen, U. Bergmann, R. Barrea, Range-extended exafs at the L edge of rare earths using high-energy-resolution fluorescence detection: A study of La in LaOCl, Phys. Rev. B 72 (2005) 014117. doi:10.1103/PhysRevB.72.014117.
URL http://link.aps.org/doi/10.1103/PhysRevB.72.014117

[17] P. Glatzel, U. Bergmann, High resolution 1s core hole X-ray spectroscopy in 3d transition metal complexes - electronic and structural information, Coord. Chem. Rev. 249 (1-2) (2005) 65–95. doi:10.1016/j.ccr.2004.04.011.

[18] A. Kotani, J. C. Parlebas, P. Le Fèvre, D. Chandesris, H. Magnan, K. Asakura, I. Harada, H. Ogasawara, Theory of hard x-ray resonant photoelectron emission and related spectra in mixed valence ce compounds, Nucl. Instr. and Meth. 547 (2005) 124.

[19] J.-P. Rueff, A. Shukla, Inelastic x-ray scattering by electronic excitations under high pressure, Rev. Mod. Phys. 82 (1) (2010) 847–896. doi:10.1103/RevModPhys.82.847.

[20] T. Vitova, K. O. Kvashnina, G. Nocton, G. Sukharina, M. A. Denecke, S. M. Butorin, M. Mazzanti, R. Caciuffo, A. Soldatov, T. Behrends, H. Geckeis, High energy resolution x-ray absorption spectroscopy study of uranium in varying valence states, Phys. Rev. B 82 (23) (2010) 235118. doi:10.1103/PhysRevB.82.235118.
URL http://link.aps.org/doi/10.1103/PhysRevB.82.235118

[21] J. P. Rueff, S. Raymond, A. Yaresko, D. Braithwaite, P. Leininger, G. Vanko, A. Huxley, J. Rebizant, N. Sato, Pressure-induced f-electron delocalization in the U-based strongly correlated compounds UPd_3 and UPd_2Al_3: Resonant inelastic x-ray scattering and first-principles calculations, Phys. Rev. B 76 (8) (2007) 085113. doi:10.1103/PhysRevB.76.085113.

[22] S. Heathman, J. P. Rueff, L. Simonelli, M. A. Denecke, J. C. Griveau, R. Caciuffo, G. H. Lander, Resonant x-ray emission spectroscopy at the L-3 edge of americium up to 23 GPa, Phys. Rev. B 82 (20) (2010) 201103. doi:10.1103/PhysRevB.82.201103.

[23] P. Söderlind, K. T. Moore, A. Landa, B. Sadigh, J. A. Bradley, Pressure-induced changes in the electronic structure of americium metal, Phys. Rev. B 84 (7) (2011) 075138. doi:10.1103/PhysRevB.84.075138.
URL http://link.aps.org/doi/10.1103/PhysRevB.84.075138

[24] S. Heathman, R. Haire, T. Le Bihan, A. Lindbaum, K. Litfin, Y. Meresse, H. Libotte, Pressure induces major changes in the nature of americium's 5f electrons, Phys. Rev. Lett. 85 (14) (2000) 2961–2964. doi:10.1103/PhysRevLett.85.2961.

[25] C. H. Booth, Y. Jiang, D. L. Wang, J. N. Mitchell, P. H. Tobash, E. D. Bauer, M. A. Wall, P. G. Allen, D. Sokaras, D. Nordlund, T.-C. Weng, M. A. Torrez, J. L. Sarrao, Multiconfigurational nature of 5f orbitals in uranium and plutonium intermetallics, Proc. Natl. Acad. Sci. U. S. A. 109 (26) (2012) 10205–10209. doi:10.1073/pnas.1200725109.

[26] J. L. Sarrao, L. A. Morales, J. D. Thompson, B. L. Scott, G. R. Stewart, F. Wastin, J. Rebizant, P. Boulet, E. Colineau, G. H. Lander, Plutonium-based superconductivity above 18 K, Nature (London) 420 (2002) 297.

[27] E. D. Bauer, M. M. Altarawneh, P. H. Tobash, K. Gofryk, O. E. Ayala-Valenzuela, J. N. Mitchell, R. D. McDonald, C. H. Mielke, F. Ronning, J.-C. Griveau, E. Colineau, R. Eloirdi, R. Caciuffo, B. L. Scott, O. Janka, S. M. Kauzlarich, J. D. Thompson, Localized 5f electrons in superconducting $PuCoIn_5$: consequences for superconductivity in $PuCoGa_5$, J. Phys.-Condes. Matter 24 (5) (2012) 052206. doi:10.1088/0953-8984/24/5/052206.

[28] P. A. Bielenberg, F. C. Prenger, D. K. Veirs, G. F. Jones, Effects of pressure on thermal transport in plutonium oxide powder, Int. J. Mass Trans. 49 (2006) 3229–3239.

[29] D. Sokaras, T. C. Weng, D. Nordlund, R. Alonso-Mori, P. Velikov, D. Wenger, A. Garachtchenko, M. George, V. Borzenets, B. Johnson, T. Rabedeau, U. Bergmann, A seven-crystal Johann-type hard x-ray spectrometer at the Stanford Synchrotron Radiation Lightsource, Rev. Sci. Instrum 84 (5) (2013) 053102. doi:10.1063/1.4803669.

[30] D. Haskel, FLUO: Correcting XANES for self absorption in fluorescence measurements (1999).
URL http://www.aps.anl.gov/xfd/people/haskel/fluo.html

[31] W. McMaster, N. D. Grande, J. Mallett, J. Hubbell, Compilation of x-ray cross sections, Tech. Rep. UCRL-50174, Lawrence Livermore National Laboratory (1969).

[32] J. Tulkki, T. Aberg, Behaviour of raman resonance scattering across the k x-ray absorption edge, Journal of Physics B: Atomic and Molecular Physics 15 (13) (1982) L435–L440. doi:10.1088/0022-3700/15/13/004.

[33] M. Taguchi, J. C. Parlebas, T. Uozumi, A. Kotani, C.-C. Kao, K β resonant x-ray emission spectra in mnf_2, Phys. Rev. B 61 (4) (2000) 2553–2560. doi:10.1103/PhysRevB.61.2553.
URL http://link.aps.org/doi/10.1103/PhysRevB.61.2553

[34] B. K. Teo, EXAFS: Basic Principles and Data Analysis, Springer-Verlag, New York, 1986, p. 74.

[35] W. Kohn, T. K. Lee, Flucuation effects in mixed-valence systems at zero temperature, Phil. Mag. A 45 (1982) 313.

[36] J. Haschke, T. Allen, L. Morales, Reaction of plutonium dioxide with water: Formation and properties of PuO2+x, Science 287 (5451) (2000) 285–287. doi:10.1126/science.287.5451.285.

[37] S. Conradson, B. Begg, D. Clark, C. den Auwer, M. Ding, P. Dorhout, F. Espinosa-Faller, P. Gordon, R. Haire, N. Hess, R. Hess, D. Keogh, G. Lander, D. Manara, L. Morales, M. Neu, P. Paviet-Hartmann, J. Rebizant, V. Rondinella, W. Runde, C. Tait, D. Veirs, P. Villella, F. Wastin, Charge distribution and local structure and speciation in the UO2+x and PuO2+x binary oxides for x ¡= 0.25, J. Solid State Chem. 178 (2, SI) (2005) 521–535. doi:10.1016/j.jssc.2004.09.029.

[38] E. Stavitski, F. M. F. de Groot, The CTM4XAS program for EELS and XAS spectral shape analysis of transition metal L edges, Micron 41 (7) (2010) 687–694. doi:10.1016/j.micron.2010.06.005.

[39] I. Josefsson, K. Kunnus, S. Schreck, A. Foehlisch, F. de Groot, P. Wernet, M. Odelius, Ab initio calculations of x-ray spectra: Atomic multiplet and molecular orbital effects in a multiconfigurational SCF approach to the L-edge spectra of transition metal complexes, J. Phys. Chem. Lett. 3 (23) (2012) 3565–3570. doi:10.1021/jz301479j.

[40] J. J. Rehr, R. C. Albers, Theoretical approaches to x-ray absorption fine structure, Rev. Mod. Phys. 72 (3) (2000) 621–654. doi:10.1103/RevModPhys.72.621.

[41] J. J. Rehr, J. J. Kas, F. D. Vila, M. P. Prange, K. Jorissen, Parameter-free calculations of X-ray spectra with FEFF9, Phys. Chem. Chem. Phys. 12 (21) (2010) 5503–5513. doi:10.1039/b926434e.

[42] W. H. Zachariasen, F. H. Ellinger, The crystal structure of alpha plutonium metal, Acta Cryst. 16 (8) (1963) 777–783. doi:10.1107/S0365110X63002012.
URL http://dx.doi.org/10.1107/S0365110X63002012

[43] F. H. Ellinger, Crystal structure of delta-prime plutonium and the thermal expansion characteristics of delta, delta-prime, and epsilon plutonium, Trans. Am. Inst. Min. Metall. Petrol. Eng. (Trans. AIME) 206 (1956) 1256–1259.

[44] J. Charvillat, D. Damien, A. Wojakowski, Cristallochimie des composes binaires $M\mathrm{Sb}_2$ et ternaires M Sb Te des elements transuraniens, Rev. Chim. Miner. 14 (14) (1977) 178–188.

[45] J. J. Rehr, J. A. Soininen, E. L. Shirley, Final-state rule vs the Bethe-Salpeter equation for deep-core X-ray absorption spectra, Physica Scripta T115 (2005) 207–211.

[46] F. Reinert, R. Claessen, G. Nicolay, D. Ehm, S. Hufner, W. Ellis, G. Gweon, J. Allen, B. Kindler, W. Assmus, Photoemission experiments on YbInCu4: Surface effects and temperature dependence, Phys. Rev. B 58 (19) (1998) 12808.

[47] S. Suga, A. Sekiyama, S. Imada, A. Shigemoto, A. Yamasaki, M. Tsunekawa, C. Dallera, L. Braicovich, T.-L. Lee, O. Sakai, T. Ebihara, Y. nuki, Kondo lattice effects of ybal3 suggested by temperature dependence of high-accuracy high-energy photoelectron spectroscopy, Journal of the Physical Society of Japan 74 (11) (2005) 2880–2884. arXiv:http://journals.jps.jp/doi/pdf/10.1143/JPSJ.74.2880, doi:10.1143/JPSJ.74.2880.
URL http://journals.jps.jp/doi/abs/10.1143/JPSJ.74.2880

[48] C. H. Booth, M. D. Walter, D. Kazhdan, Y.-J. Hu, W. W. Lukens, E. D. Bauer, L. Maron, O. Eisenstein, R. A. Andersen, Decamethylytterbocene Complexes of Bipyridines and Diazabutadienes: Multiconfigurational Ground States and Open-Shell Singlet Formation, J. Am. Chem. Soc. 131 (18) (2009) 6480. doi:10.1021/ja809624w.

[49] F. Bridges, C. H. Booth, M. Anderson, G. H. Kwei, J. J. Neumeier, J. Snyder, J. Mitchell, J. S. Gardner, E. Brosha, Mn K-edge XANES studies of $\mathrm{La}_{1-x}A_x\mathrm{MnO}_3$ systems (A = Ca, Ba, Pb), Phys. Rev. B 63 (2001) 214405. doi:10.1103/PhysRevB.63.214405.

[50] J.-X. Zhu, P. H. Tobash, E. D. Bauer, F. Ronning, B. L. Scott, K. Haule, G. Kotliar, R. C. Albers, J. M. Wills, Electronic structure and correlation effects in PuCoIn_5 as compared to PuCoGa_5, EPL 97 (5) (2012) 57001. doi:10.1209/0295-5075/97/57001.

[51] M. E. Pezzoli, K. Haule, G. Kotliar, Neutron magnetic form factor in strongly correlated materials, Phys. Rev. Lett. 106 (2011) 016403. doi:10.1103/PhysRevLett.106.016403.

[52] C. H. Booth, E. D. Bauer, M. Daniel, R. E. Wilson, J. N. Mitchell, L. A. Morales, J. L. Sarrao, P. G. Allen, Quantifying structural damage from self-irradiation in a plutonium superconductor, Phys. Rev. B 76 (6) (2007) 064530. doi:10.1103/PhysRevB.76.064530.

[53] M. J. Fluss, B. D. Wirth, M. Wall, T. E. Felter, M. J. Caturla, A. Kubota, T. Diaz de la Rubia, Temperature-dependent defect properties from ion-irradiation in Pu(Ga), J. Alloys Compd. 368 (2004) 62.

[54] S. K. McCall, M. J. Fluss, B. W. Chung, M. W. McElfresh, D. D. Jackson, G. F. Chapline, Emergent magnetic moments produced by self-damage in plutonium, Proc. Natl. Acad. Sci. U.S.A. 103 (2006) 17179.

[55] C. H. Booth, Y. Jiang, S. A. Medling, D. L. Wang, A. L. Costello, D. S. Schwartz, J. N. Mitchell, P. H. Tobash, E. D. Bauer, S. K. McCall, M. A. Wall, P. G. Allen, Self-irradiation damage to the local structure of plutonium and plutonium intermetallics, J. Appl. Phys. 113 (9) (2013) 093502. doi:10.1063/1.4794016.

[56] J. C. Lashley, J. Singleton, A. Migliori, J. B. Betts, R. A. Fisher, J. L. Smith, R. J. McQueeney, Experimental electronic heat capacities of α- and δ-plutonium: Heavy-fermion physics in an element, Phys. Rev. Lett. 91 (20) (2003) 205901. doi:10.1103/PhysRevLett.91.205901.

[57] J. C. Lashley, A. Lawson, R. J. McQueeney, G. H. Lander, Absence of magnetic moments in plutonium, Phys. Rev. B 72 (5) (2005) 054416. doi:10.1103/PhysRevB.72.054416.

[58] P. Javorský, E. Colineau, F. Wastin, F. Jutier, J.-C. Griveau, P. Boulet, R. Jardin, J. Rebizant, Specific heat and anisotropy of the nonconventional superconductors PuCoGa_5 and PuRhGa_5, Phys. Rev. B 75 (18) (2007) 184501. doi:10.1103/PhysRevB.75.184501.

[59] S. K. McCall, private communication.